Deployment of Energy-Efficient Aerial Communication Platforms with Low-Complexity Detection

Mingze Zhang, *Student Member, IEEE,* Yifeng Xiong, *Student Member, IEEE,*
Soon Xin Ng, *Senior Member, IEEE,* and Mohammed El-Hajjar, *Senior Member, IEEE*

***Abstract*—Due to their flexibility, mobility and autonomy, unmanned aerial vehicles (UAVs) are considered as a potential candidate to operate as flying base stations to provide a specific geographical area with air-to-ground wireless communications services. Besides, the limitation of the on-board energy motivates the design of a more energy-efficient way to transmit information. Moreover, the deployment of multiple UAVs can affect the quality of experience (QoE) of users. In this paper, we propose a method that combines the concept of index modulation (IM) with the UAV communications systems, which we refer to as IM-UAV, to attain an improved energy-efficiency (EE). Furthermore, based on the proposed IM-UAV communication system, a gradient descent based UAV deployment scheme is designed to maximize the downlink average rate of the ground users (GUs) in the target area. On the other hand, the maximum likelihood (ML) detection for the IM-UAV requires a high computational complexity for detection at the GUs, while providing the best possible performance. Hence, we propose a low-complexity detection scheme that can separately detect the index symbols and data symbols to reduce the computational complexity at the receiver side. The simulation results demonstrate that the proposed deployment method is capable of attaining the appropriate positions to deploy the UAVs, while the EE is also improved by combining IM with UAV communication system. In addition, the proposed low-complexity detection scheme reduces the computation complexity by slightly sacrificing the bit error rate (BER) performance.**

***Index Terms*—UAV, index modulation, MIMO, OFDMA, deployment, energy-efficiency, detection.**

I. Introduction

THERE has been an explosive growth in the use of unmanned aerial vehicles (UAVs) in the past decade [1], [2]. Due to this significant increase in the number of UAVs, innovative utilization of these vehicles is emerging including in telecommunications [3]. Given their flexibility, maneuverability and their reducing cost, a wide range of applications can be performed by UAVs such as aerial inspection, smart logistic, precision agriculture, disaster response and package delivery [4]–[7]. All these UAV-assisted applications, which support ground users (GUs) as well as existing terrestrial infrastructures and communication entities, is experiencing significantly increased research interest [8]. Meanwhile, wireless communication is essential to support a wide range of applications, including the above-mentioned examples. On one hand, UAVs need the control and non-payload communication to adjust their flight by exchanging safetycritical information with various parties [9], [10]. On the other hand, UAVs may have to transmit or receive mission related data such as image, video and data, which is also known as payload communication [11]. Additionally, the UAVs can be considered as user equipment or aerial base station (BS) in cellular networks [12].

The high altitude of UAVs can provide line of sight (LoS) dominant air to ground (A2G) communication channels [13], which enables wider ground coverage and strong communication links. However, compared to the traditional terrestrial counterparts that has stable power supply from the power grid, the size, weight and power constraints of UAVs results in new design challenges of integrating UAVs to the existing cellular networks.

A. UAV Deployment

Among all challenges brought by integrating UAVs to cellular networks, the deployment of UAVs is a challenging task, that should be carefully considered. The authors of [14] considered the deployment of UAVs as a placement game to minimize the social service cost, while the work in [15] analyzed the deployment of UAVs from the perspective of dynamic service pricing, which aims to maximize the total UAV-provided service profit. On the other hand, an optimization model to minimize the system power consumption by applying dual decomposition method was proposed in [16], where the UAV deployment and transmission power were jointly optimized. Also, a number of k-means clustering-based multiple UAV deployment schemes were proposed in [17], [18]. In [19], the authors proposed an adaptive deployment scheme to adjust its location based on the instantaneous traffic load of moving users in different sectors within its target cell. Besides, the authors of [20] systematically reviewed the real-time deployments of UAV-based long-range communication network. Furthermore, in [21], the authors formulated the learning-and-adaptation based deployment problem as a partially observable Markov decision process to maximize the total discounted hit rate of active users. Additionally, the authors of [22] proposed a 3-D deployment approach to maximize the minimum achievable system throughput for all GUs by considering the co-channel interference. Moreover, due to the advancement in artificial intelligence, the authors

The authors are with the School of Electronics and Computer Science, University of Southampton, Southampton SO17 1BJ, United Kingdom (email:{mz6u17,yx8n18,sxn,meh}@ecs.soton.ac.uk).

of [23]–[25] utilized deep learning in the deployment of UAVs with different target functions.

B. Energy-Efficiency of UAV

The performance of UAV communication system is fundamentally limited by the on-board energy, which is closely related to the size and weight of the UAVs [26]. The total power consumption of a UAV includes two components. The first one is the communication-related energy, which is consumed by the radiation, signal processing and other circuitry. While the rest is the propulsion energy required for hovering as well as for supporting its mobility [2]. In [27], the authors proposed an optimal deployment framework for minimizing the total required transmission power of UAVs while satisfying the GUs' rate requirements in a downlink scenario. The authors of [28] derived a energy consumption model of fixed-wing UAV according to the trajectory of UAV, based on which the EE of UAV communication is defined, but the communication-related energy was ignored in this work. Afterwards, the authors of [29] jointly optimized the scheduling scheme, power allocation strategy and flight trajectory of the UAV based on the energy consumption model of [28], which aims to minimize the total power consumption of the UAV. The authors of [30] proposed a multi-UAV coverage deployment model in a UAV network with game-theoretic framework, where a UAV coverage scenario was built to solve the problem of energy shortages. Similarly, the energy consumption model of rotary-wing UAV has been derived in [31] to minimize the total UAV energy consumption, while the communication-related energy was considered as a constant. Besides, a new energy consumption model considering both acceleration and deceleration as a function of acceleration and time duration has been derived in [32], which is also a modification of [31]. According to [31], the works of [33] studied the energy-time trade-off for the rotary-wing UAV enabled wireless-powered communication network, while satisfying the communication throughput requirement for each GU. However, another kind of propulsion energy consumption model that divides the total power consumption of UAV flight into moving energy consumption and hovering energy consumption was considered in [34], while the communication-related energy consumption was assumed to be a constant. In addition, an energy-efficient radio resource management optimization framework for UAV-assisted millimeter wave 5G heterogeneous cellular networks was studied in [35]. Moreover, the authors of [36] minimized the energy consumption in a UAV-assisted mobile edge computing system by jointly optimizing the UAV trajectory and computation resource allocation, where a modified propulsion energy consumption model similar to [28] and [31] has been taken into account. Furthermore, the works of [37] has provided a new optimization framework for a UAV-aided network, which combines the ambient backscatter communication with non-orthogonal multiple access to minimize the total power consumption under imperfect channel state information.

C. Index Modulation for UAV

The concept of index modulation (IM), which is capable of enhancing the systems energy-efficiency (EE) and providing high-rate data transmission, has become a promising technique for wireless communications [38]. It can be applied in space domain, frequency domain and time domain with high EE and SE [39]. Besides, IM has been proposed to reduce the complexity in the future generation wireless networks due to its flexible system structure [40]. In IM-aided systems, in addition to the symbol bits carried by conventional amplitude or phase modulation, extra information bits are conveyed by the indices of activated transmit entities, without extra energy consumption [41].

In [42], a UAV-aided communication system that combines orthogonal frequency division multiplexing (OFDM) with IM is established to achieve a trade-off between SE and bit error rate (BER) performance. In this work, the authors combine the UAV with OFDM-IM without utilizing the benefits of using UAVs in an IM scenario. The multiple UAVs in this OFDM-IM scenario were individually considered as independent BSs with no cooperation between them. Also, the deployment issue of multiple UAVs has not been considered in this work, which can be further investigated. Moreover, another kind of IM-based UAV communication system that combines spatial modulation (SM) with UAVs was proposed in [43], where the authors considered one UAV as a half-duplex relay with amplify-and-forward protocol in an imperfect channel state information (CSI) scenario. However, in [43] only one UAV was considered and the concept of SM was applied in the UAV. The authors of [44] invoked the coherent/non-coherent SM and its diversity-oriented counterpart of space-time block coding using index shift keying to achieve a significant quality of service (QoS), where a fixed wing UAV was employed, which is incapable of hovering at one particular location. In addition, a space shift keying modulation based UAV communication system was proposed in [45] to achieve reliable and EE communication links. Similar to [42], the authors analyzed two scenarios: UAV to ground BS and UAV to UAV communications, where the UAVs are all working as independent BSs. Recently, the works of [46] investigated the grant-free non-coherent IM scheme combined with OFDM for applicant to UAV-based massive Internet-of-things (IoT) access. In this work, both fixed-wing UAV and rotary-wing UAV were considered based on their payload capacities. However, the IM was still utilized for tackling the issues of low-cost and low-energy consumption for massive IoT access without any combination of UAV properties. Besides, only one UAV was employed as an aerial BS to serve GUs and the deployment of UAV has not been clearly demonstrated.

D. Motivation and Contribution

In the aforementioned IM-UAV related works, IM was not directly related to UAVs but simply employed in the aerial communication platform, which means the UAVs themselves have no connection with the index bits. Besides, the cooperation among multiple IM-based UAVs has not been discussed. Meanwhile, the works mentioned above mainly consider one-to-one communication, while one-to-many or many-to-many communication has not been deeply investigated. Additionally, the deployment of UAV or UAVs has not been thoroughly

explored in these works. Therefore, a deeper combination of multiple UAVs and IM needs to be studied, where the UAVs are connected to the index bits. Then, the deployment of multiple UAVs need to be considered in order to improve the quality of experience (QoE) of GUs in the IM scenario. To the best of our knowledge, the specific transmission energy consumption model in multiple IM-UAV communication system with UAV cooperation has not been investigated, and the EE of IM-UAV communication need to be analyzed. Moreover, one of the most significant challenges in IM related systems is the need for low-complexity detection, which is also a key element when considering the limited resources available at the receiver side.

Against this background, in this paper we propose to use UAVs as flying BSs to increase the probability of having LoS communication links. Meanwhile, in order to support multiple GUs simultaneously and alleviate the performance degradation caused by the multipath channel fading of the non line of sight (NLoS) propagation, we employ orthogonal frequency-division multiple access (OFDMA) techniques. Furthermore, due to the power limitation of UAVs, it is important to design energy-efficient transmission schemes, and hence we combine the concept of IM with UAV communications to establish an IM-UAV communication system, which treats the activated UAV as index to separately send data bits by conventional data symbols and using the index information. Besides, the deployment of UAVs will also affect the QoS of GUs, hence we propose a gradient descent based deployment algorithm to maximize the downlink sum rate of GUs in the target area. Moreover, the optimal maximum likelihood (ML) detection that can provide the best BER performance, requires a high detection complexity. Consequently, a low-complexity detection scheme is required to reduce the detection computational complexity at the receiver side. Hence, our contributions can be summarized as follows:

1) Inspired by the index modulation scheme and its potential for high EE, we propose a novel IM-UAV communication network, where UAVs are employed as flying BSs to establish stable and reliable A2G communication links. More specifically, for different subcarrier, different combinations of UAVs are activated based on the input index bits.
2) We use OFDMA for the multi-user communications, where each GU will be assigned to their corresponding subcarriers using OFDMA. Furthermore, only those activated UAVs will modulate data symbols onto their corresponding subcarriers and transmit OFDM symbols to all GUs simultaneously.
3) Moreover, we successfully derive the gradient of the sum rate in the scenario of our proposed IM-UAV communication network with respect to the positions of UAVs. Since the location of GUs and the location of UAVs are linked together, UAVs are capable of adaptively finding out the position, where the maximum rate can be achieved, by following the obtained gradient, regardless of the distribution of GUs on the ground.
4) Finally, in order to reduce the high complexity required for the optimal ML detection, we propose a new detection scheme according to the transmission characteristics of the proposed IM-UAV system. By utilizing the feature of path loss in A2G communication links that exists in our proposed communication system and the properties of constellation symbols, the proposed detection scheme is able to separately detect the index symbols and the conventional data symbols based on the strength and the phase of the received signals. Instead of searching each possible combination step by step, detecting the phase and the amplitude of the received signals can be used to filter part of the combinations, which reduces the detection complexity but sacrifices slightly the BER performance.

The rest of this paper is organized as follows. In Section II, we present the system model of proposed IM-UAV communication system. Afterwards, we analyze our simulation results in Section III followed by our conclusions in Section IV.

II. IM-UAV Communication System

In this paper, we consider a UAV-assisted downlink communication network in a target area, where N_d UAVs are deployed to operate as aerial BSs and each equipped with one transmitter (Tx) antenna to provide wireless communication services to GUs in this area as shown in Fig. 1. We assume that these N_d UAVs are capable of flying horizontally and hovering at a certain altitude of h_d [47]. In this scenario, UAVs can periodically exchange their location information by air to air (A2A) communciation links [48], [49]. Meanwhile, both OFDMA and SM techniques have been employed to support the A2G communication links between UAVs and GUs simultaneously, as will be detailed later.

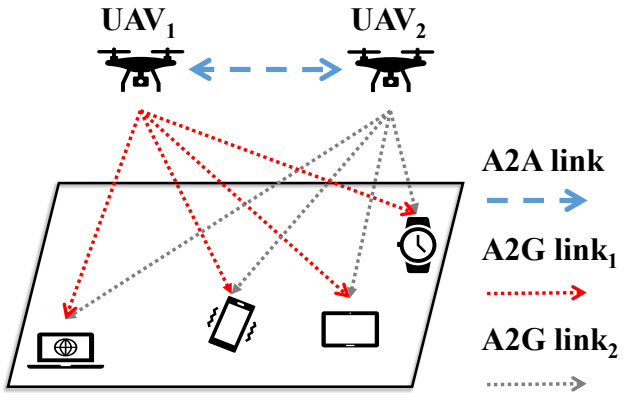

Fig. 1: UAV-assisted network model that provides service of wireless communication for GUs.

In the conventional SM, a set of information bits is mapped to a constellation symbol and a spatial symbol. The spatial symbol is utilized to select one combination of activated transmit antennas from all possible combinations at each time slot. Here, the actual combination of active transmit antennas depends on the random incoming data bits [50]. However, in our proposed IM-UAV system, the function of the index bits is different as detailed in the following section. Since OFDMA is implemented in our system to realise multi-user communication, the bandwith resources is divided into small

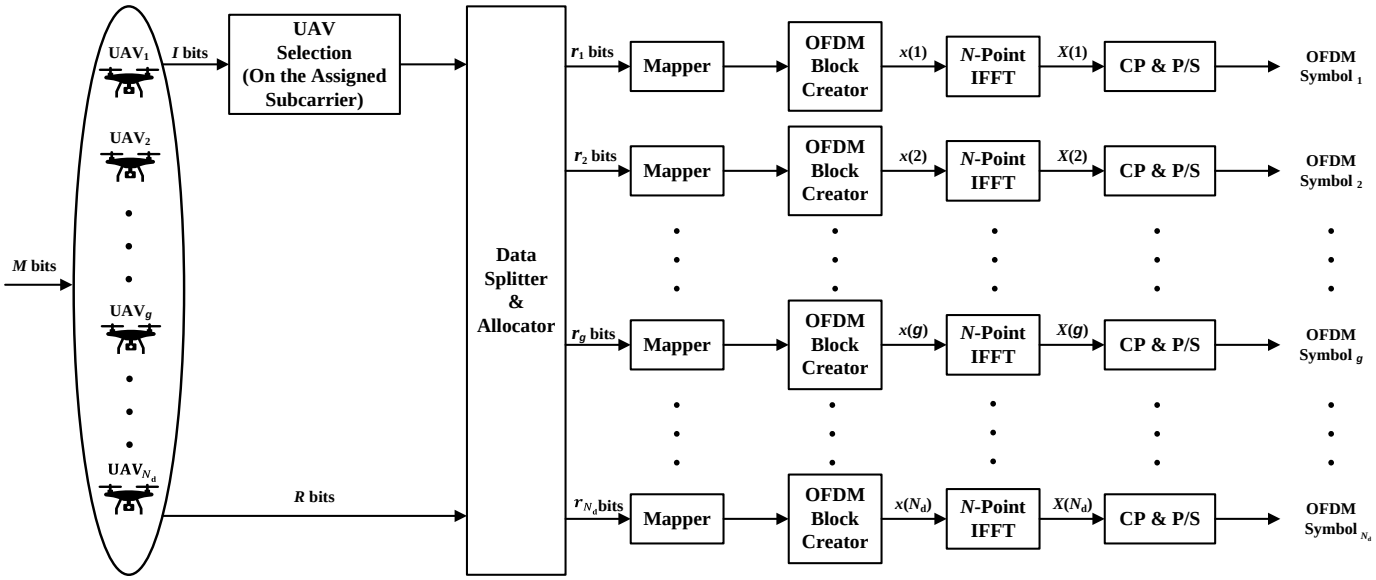

Fig. 2: Block diagram of the IM-UAV transmitter.

units (subcarriers), which are assigned to GUs according to their real-time requirements [51]–[53]. In the proposed system, the indices are utilised to select the UAVs that will be used to modulate the constellation symbols onto those pre-allocated subcarriers.

As shown in Fig. 2, all GUs are served by all UAVs in our system and each GU will be assigned their corresponding subcarrier by using OFDMA scheme. Firstly, the $\boldsymbol{M}$ incoming data bits of all GUs are shared by all UAVs, which will be divided into two parts: the index part that has $\boldsymbol{I}$ bits used to select the transmitting UAVs per subcarrier and the remaining $\boldsymbol{R}$ data bits are used to map to the conventional modulation symbols, such as quadrature phase-shift keying (QPSK). Since all the UAVs are working together to serve all the GUs, the UAVs will use these $\boldsymbol{I}$ bits to correspondingly activate themselves on the assigned subcarriers of the GUs. Then, according to those activated UAVs on the assigned subcarriers, the remaining $\boldsymbol{R}$ bits will be split and mapped onto constellation symbols as shown in Fig. 2. It is worth noting that the number of constellation symbols assigned to each UAV can be different but the total number of bits transmitted satisfy the constraint:

$$\boldsymbol{R} = \boldsymbol{r}_1 + \boldsymbol{r}_2 + \ldots + \boldsymbol{r}_g + \ldots + \boldsymbol{r}_{N_d}, \tag{1}$$

where $\boldsymbol{r}_g$ corresponds to the bits transmitted from the g^{th} UAV. Afterwards, each UAV will generate a OFDM block based on its assigned constellation symbols. After this point, each frequency domain OFDM symbol $\boldsymbol{x}(g)$ will be transferred to time domain block $\boldsymbol{X}(g)$ using the inverse fast Fourier transform (IFFT) as depicted in Fig. 2, where $g \in [1, 2, \ldots, N_d]$. At the output of the IFFT, cyclic prefix (CP) is appended to each OFDM block [54]. It is worth noting that all these aforementioned steps happen at all UAVs in our system as depicted in Fig. 2.

In the following, we will explain the "OFDM block creator" processing of Fig. 2 in the transmitter of the proposed IM-UAV system using the example shown in Fig. 3. In this specific example, we consider employing 4 UAVs and 8 subcarriers indicated by the boxes in Fig. 3. For simplicity, we assume that each GU is assigned one subcarrier, thus, totally 8 GUs are served by all 4 UAVs. In this case, only one UAV is activated at a time in the frequency domain. Hence, 2 bits are required for the selection of UAVs. Additionally, we assume data symbols are modulated using QPSK. Therefore, totally 4 bits are needed for the selection of UAV and the modulation of data symbols for each subcarrier. Here, we assume the incoming information bits requested by each GU on their assigned subcarriers are $(0011, 1001, 1101, 1010, 0000, 1110, 0111, 0100)$[1] and all these information will be shared by A2A links among all UAVs to control the modulation scheme [48], [49]. As shown in Fig. 3, each UAV is indexed by binary number sequence. Besides, the first two bits of each data bits block marked by red color are used to select one of the UAVs. In each column of boxes, only the corresponding box of the activated UAV is outlined by red. For instance, the data for the first GU in the above example is "0011". Here, we have "00" to indicate the UAV index and "11" for the symbol, which means the first subcarrier is occupied by the first UAV and the following two data bits "11" will be mapped to their constellation symbols and carried by this subcarrier. Again, the four boxes in each column in the illustration of Fig. 3 are to indicate which UAV will occupy this subcarrier. Afterwards, each UAV has its own OFDM block in the frequency domain followed by the classical OFDM procedures [55]. In the following, we will present the channel model followed by the deployment of IM-UAV communication and then a modified power consumption model and a low-complexity detection scheme will be presented.

[1] Here, each four-bit sequence corresponds to one GU.

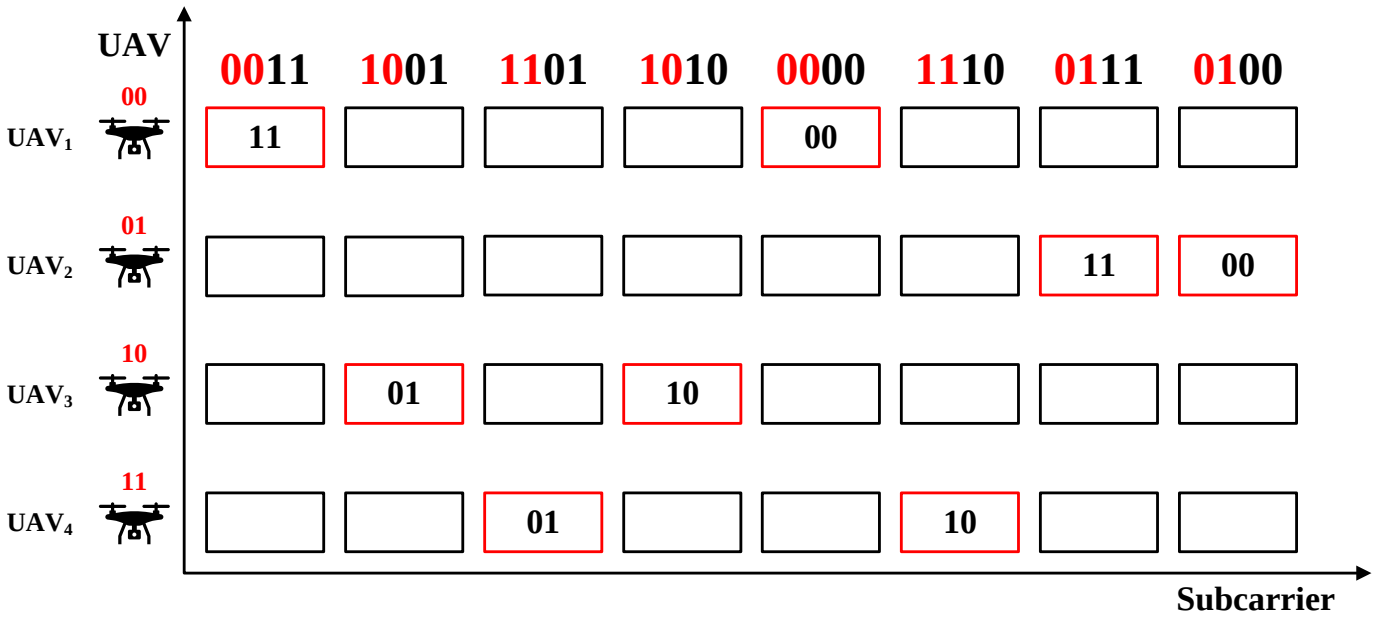

Fig. 3: Illustration of the IM-UAV block creator using 4 UAVs, 8 RUs and QPSK modulation scheme in the frequency domain.

A. Channel Model

Given that the UAVs are considered as aerial BSs to serve GUs, the communication between GUs and UAVs is in strong LoS propagation environment [56]. The strong LoS is usually considered as a cause of low rank channel matrix in MIMO communication system, which brings correlation among MIMO channels, which reduces the capability of supporting multiple parallel data streams. However, those aerial BSs or UAVs are separately deployed in a target area and it gives enough space to reduce the correlations. According to [57], the channel is largely determined by the distance between the transmitter (UAV) and the receiver (GU) in a LoS environment, since the UAVs are usually separately deployed when in operation and hence the distances from each UAV to the same GU end is different most of the time. Therefore, this will lead to phase differences between different channels as will be detailed in the following. In other words, the receiver side is able to clearly distinguish between different signals from different UAVs.

We consider a downlink MIMO scenario, where each UAV is equipped with one Tx antenna and totally $N_t = N_d$ antennas employed at the transmitter side, which is comprised on the joint UAVs forming a virtual MIMO. Also, N_r receiver (Rx) antennas are employed at each GU and a frequency-flat channel is assumed on the subcarriers due to the OFDMA technique [55]. Hence, the received signal in the frequency domain can be expressed as [58]:

$$\boldsymbol{y} = \sqrt{P_t}\boldsymbol{H}\boldsymbol{x} + \boldsymbol{v}, \tag{2}$$

where $\boldsymbol{x}$ denotes the N_t-dimensional transmitted symbol vector, while $\boldsymbol{y}$ denotes the N_r-dimensional received symbol vector. $\boldsymbol{H}$ indicates the $N_r \times N_t$ channel matrix, where each element h_{ij} represents the channel from the j^{th} transmitter antenna to the i^{th} receiver antenna, for $i = 1, 2, \ldots, N_r$ and $j = 1, 2, \ldots, N_t$. $\boldsymbol{v}$ is the N_r-dimensional independent identically distributed (i.i.d) zero-mean complex Gaussian noise vector with covariance matrix $\boldsymbol{I}_{N_r}$. P_t is the achievable transmission power at each Tx antenna over a transmission interval.

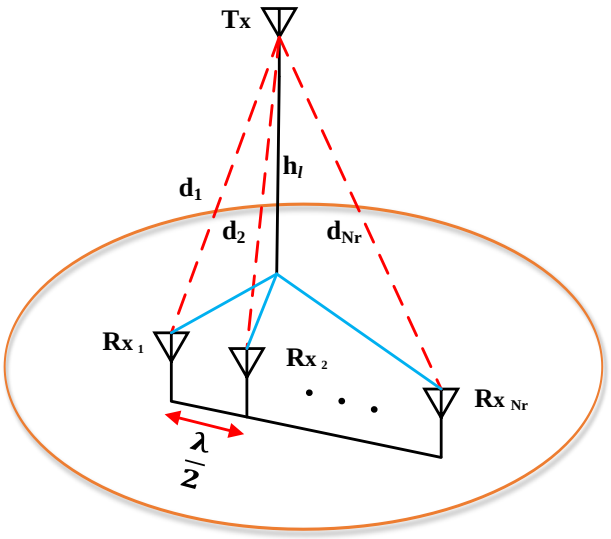

Fig. 4: Illustration of A2G distances with one aerial Tx antenna and N_r ground Rx antennas of a ULA.

The Rician MIMO channel is employed in our A2G communication as it decomposes the channel into two parts [59]: deterministic LoS component $\boldsymbol{H}_{\text{LoS}}$ and stochastic NLoS component $\boldsymbol{H}_{\text{NLoS}}$. The NLoS component is used for scattered multipath propagation of signals and the Rician K factor is the ratio of the power of the two components [60]. Hence, the channel matrix $\boldsymbol{H}$ is given by:

$$\boldsymbol{H} = \sqrt{\frac{K}{K+1}} \cdot \boldsymbol{H}_{\text{LoS}} + \sqrt{\frac{1}{K+1}} \cdot \boldsymbol{H}_{\text{NLoS}}. \tag{3}$$

Accordingly, in the condition of A2G transmission in our UAV-aided communication system, a relatively large value of K, which ranges from 0.51 to 6.31 [61], will be considered to generate a LoS-dominant channel. The LoS component of $\boldsymbol{H}$ is determined by the LoS distances between the UAV and the GU. A model with 1 Tx antenna and N_r Rx antennas is illustrated by Fig. 4, where the vertical distance from air to ground is h_d and the coordinate of the Tx antenna is assumed to be (x_t, y_t, h_d). Besides, the Rx antennas at the GU on the ground is considered as a uniform linear array (ULA) [62], which means all antennas are uniformly distributed with an interval of $\frac{\lambda}{2}$ where λ is the wavelength of the carrier. For simplicity, we assume that the coordinate of the first Rx antenna is (x_r, y_r) as the height of Rx antenna is negligible compared with the A2G distance. As depicted by Fig. 4, the coordinates of the n_r^{th} Rx antenna can be represented by $(x_r + \frac{\lambda(n_r-1)}{2}, y_r)$, where $n_r \in [1, 2, \ldots, N_r]$ is the index of the Rx antenna.

Finally, the distance between the Tx antenna and the n_r^{th} Rx antenna is given by:

$$d_{n_r} = \sqrt{(x_t - x_r - \frac{\lambda(n_r-1)}{2})^2 + (y_t - y_r)^2 + h_d^2}. \quad (4)$$

The LoS component vector in this example from the UAV antenna can be expressed by [57]:

$$\boldsymbol{H}_{\text{LoS}} = \left[e^{-j\frac{2\pi}{\lambda}d_1}, e^{-j\frac{2\pi}{\lambda}d_2}, \ldots, e^{-j\frac{2\pi}{\lambda}d_{N_r}}\right]^T, \quad (5)$$

where $(\cdot)^T$ denotes the transpose. Afterwards, the NLoS part of the channel $\boldsymbol{H}_{\text{NLoS}}$ is caused by multipath propagation, which can be described by Rayleigh fading channel. Therefore, the channel $\boldsymbol{H}$ in (3) can be obtained by adding the LoS part and the NLoS part together, while the K factor that indicates the ratio between them is used to describe the channel condition.

Besides, the path loss is commonly considered in A2G communication system, which is closely linked with the environment, where the Tx and Rx are operating [63]. In general, the propagation path loss P_l is expressed by [64], [65]:

$$P_l = \left(\frac{4\pi}{\lambda}\right)^2 d^{\alpha}, \quad (6)$$

where d is the distance between the Tx and Rx, the path loss exponent α ranges from 2 to 6 and the free space wavelength $\lambda = \frac{c}{f_c}$ is defined as the ratio of the speed of light c in m/s to the carrier frequency f_c in Hz. Therefore, the received signal power P_r given a transmission power P_t is formulated by [66]:

$$P_r = \frac{P_t}{P_l} = P_t \left(\frac{c}{4\pi f_c}\right)^2 \left(\frac{1}{d}\right)^{\alpha}. \quad (7)$$

In our IM-UAV communication system, the UAVs are considered to work at a height of 100 m [67] and the LoS communication links are assumed to exist for most of the time [56]. Hence, free space path loss exponent $\alpha = 2$ is chosen to describe the signal attenuation [68] and P_r is transformed to:

$$P_r = P_t \left(\frac{c}{4\pi d f_c}\right)^2. \quad (8)$$

Additionally, the transmission scheme in our proposed IM-UAV communication network is a downlink MIMO system with distributed Tx antennas as we assume each UAV will use one TX antenna to transmit data symbols simultaneously in each transmission interval. Therefore, the signal $\boldsymbol{y}$ received by one GU is given by:

$$\boldsymbol{y} = \sqrt{\boldsymbol{P}_r}\boldsymbol{H}\boldsymbol{x} + \boldsymbol{v}, \quad (9)$$

where the signal power $\boldsymbol{P}_r$ at the receiver side is a diagonal matrix in the form of:

$$\boldsymbol{P}_r = \begin{bmatrix} p_{r1} & 0 & \cdots & 0 \\ 0 & p_{r2} & \cdots & 0 \\ \vdots & \vdots & \ddots & \vdots \\ 0 & 0 & \cdots & p_{rN_t} \end{bmatrix}. \quad (10)$$

B. UAV Deployment for the IM-UAV Communication System

In a UAV-assisted communication system, it is important to utilise the maneuverability and flexibility of UAVs, which cannot be realised in traditional fixed BSs, to further improve the QoE of GUs. Therefore, we design a new deployment scheme to improve the sum rate of GUs in the context of our proposed IM-UAV communication system. Since the channel model of our IM-UAV communication has been provided, the capacity related to this channel can be formulated. When evaluating the capacity of the conventional MIMO systems, the transmitted vector $\boldsymbol{x}$ is assumed to be a zero-mean complex Gaussian random vector [69], which is able to maximize the mutual information between the transmitted and received vectors. Additionally, the normalized transmitted vector $\boldsymbol{x}$ is subject to the power constraint [69]–[71]:

$$Tr\left(E\left[\boldsymbol{x}\boldsymbol{x}^H\right]\right) \leq 1, \quad (11)$$

where $(\cdot)^H$ denotes the conjugate transpose.

On the other hand, consider the multiple data streams defined as $\boldsymbol{s} = [s_1, s_2, \ldots, s_{N_a}]^T$ that satisfy the unity power constraint, where N_a is the number of activated UAVs, and the form of transmitted vector $\boldsymbol{x}$ is given by [72]:

$$\boldsymbol{x} = \boldsymbol{Q}\boldsymbol{s}, \quad (12)$$

where $\boldsymbol{Q} \in \mathbb{C}^{N_t \times N_a}$ such that $\boldsymbol{Q} \in \mathcal{Q} = \left\{\boldsymbol{Q}_1, \boldsymbol{Q}_2, \ldots, \boldsymbol{Q}_{K_{N_a}}\right\}$ and K_{N_a} depends on the structure of the activated UAVs, which is the number of all possible combinations. For example, when considering the example of employing four UAVs and activating one UAV based on the index modulation, then there are $K_{N_a} = 4$ possible combinations that can be represented by:

$$\begin{bmatrix} 1 & 0 & 0 & 0 \\ 0 & 1 & 0 & 0 \\ 0 & 0 & 1 & 0 \\ 0 & 0 & 0 & 1 \end{bmatrix}, \quad (13)$$

where $\{\boldsymbol{Q}_1, \boldsymbol{Q}_2, \boldsymbol{Q}_3, \boldsymbol{Q}_4\}$ correspond to the rows of (13). Moreover, the power constrain in (11) makes the $\boldsymbol{x}$ satisfy the condition:

$$Tr\left(E\left[\boldsymbol{Q}_i\boldsymbol{s}\boldsymbol{s}^H\boldsymbol{Q}_i^H\right]\right) \leq 1. \quad (14)$$

The matrix set $\mathcal{Q}$ can be mapped to a set of covariance matrix $\mathcal{V} = \left\{\boldsymbol{V}_1, \boldsymbol{V}_2, \ldots, \boldsymbol{V}_{K_{N_a}}\right\}$. For instance, in the case of fixed

N_a number of data streams, the i^{th} covariance matrix of the transmitted vector can be written as:

$$\begin{aligned}\boldsymbol{V}_i &= E\left[\boldsymbol{x}\boldsymbol{x}^H|\boldsymbol{Q}=\boldsymbol{Q}_i\right]\\ &= E\left[\boldsymbol{Q}_i\boldsymbol{s}\boldsymbol{s}^H\boldsymbol{Q}_i^H\right]\\ &= \boldsymbol{Q}_i\boldsymbol{Q}_i^H,\end{aligned} \tag{15}$$

for $i = 1, 2, \ldots, K_{N_a}$, where $\boldsymbol{V}_i$ is the covariance of the transmitted vector $\boldsymbol{x}$ by assuming that $\boldsymbol{s}$ has complex Gaussian i.i.d. entries with zero mean and unit variance. This covariance matrix $\boldsymbol{V}_i$ is related to the achievable rate, which will be used in the following section to calculate the gradient of the achievable rate and deploy the UAVs in the target area.

Based on (15) the lower bound of the achievable rate is given by [72]:

$$\begin{aligned}R_L^M = -\frac{1}{K_{N_a}}\log\left(\prod_{i=1}^{K_{N_a}}\left(\sum_{j=1}^{K_{N_a}}\frac{1}{\pi^{N_r}|\boldsymbol{\Sigma}_i+\boldsymbol{\Sigma}_j|}\right)\right)\\ +\log K_{N_a} - N_r\log\left(\pi e\right),\end{aligned} \tag{16}$$

where $|\cdot|$ indicates the determinant operation, $\boldsymbol{\Sigma}_i = \rho\boldsymbol{H}\boldsymbol{V}_i\boldsymbol{H}^H + \boldsymbol{I}_{N_r}$ for $i = 1, 2, \ldots, K_{N_a}$, where ρ is the signal to noise ratio and $\boldsymbol{I}_{N_r}$ is the N_r-dimensional identity matrix. It can be found that when the structure of the transmission is defined, the element which will affect R_L^M is $\boldsymbol{H}$. As stated in the previous section, the path loss has a steady and significant impact on $\boldsymbol{H}$, which is mainly determined by the distance between the Tx and the Rx. Meanwhile, the locations of the GUs affect the A2G distances, which is related to the path loss. Therefore, the gradient of the achievable rate of GUs can be obtained by taking the derivative of R_L^M with respect to the coordinates (location) of the GUs, then the value of the achievable rate can be optimized by following the gradient descent approach [73].

Firstly, the UAVs will take the derivative of R_L^M with respect to channel $\boldsymbol{H}$ based on the information of GUs location they collected. Here, since we consider a LoS dominant environment, the channel condition or the received signal power is largely dependent on the distance between GUs and UAVs. Even if there is a small NLoS component existing in the channel, we cannot exactly find the relation between the distance and the received signal as it is totally random and uncontrollable. Therefore, we take the derivative of $\boldsymbol{H}_{\text{LoS}}$ instead of $\boldsymbol{H}$ as an approximation to optimize the deployment of UAVs. Then, in the rest of this section we use $\boldsymbol{H}$ to denote the LoS component. Here, the derivative of $\boldsymbol{H}$ with respect to the A2G distance $\boldsymbol{D}$ between the UAVs and the GUs will be obtained. Afterwards, the derivative of $\boldsymbol{D}$ with respect to the coordinates (location) of UAVs will be calculated. Finally, the derivative of R_L^M with respect to the coordinates (location) of UAVs can be obtained based on the chain rule.

Then, the derivative of R_L^M with respect to $\boldsymbol{H}$ can be obtained as:

$$\begin{aligned}d\left(R_L^M\right) &= -K_M^{-1}d\left[\log\left(\prod_{i=1}^{K_{N_a}}\left(\sum_{j=1}^{K_{N_a}}\frac{1}{\pi^{N_r}|\boldsymbol{\Sigma}_i+\boldsymbol{\Sigma}_j|}\right)\right)\right]\\ &= -K_{N_a}^{-1}\sum_{i=1}^{K_{N_a}}\frac{d\left(\sum_{j=1}^{K_{N_a}}|\boldsymbol{\Sigma}_i+\boldsymbol{\Sigma}_j|^{-1}\right)}{\sum_{j=1}^{K_{N_a}}|\boldsymbol{\Sigma}_i+\boldsymbol{\Sigma}_j|^{-1}}\\ &= -K_{N_a}^{-1}\sum_{i=1}^{K_{N_a}}\frac{\sum_{j=1}^{K_{N_a}}\left[-|\boldsymbol{\Sigma}_i+\boldsymbol{\Sigma}_j|^{-2}d\left(|\boldsymbol{\Sigma}_i+\boldsymbol{\Sigma}_j|\right)\right]}{\sum_{j=1}^{K_{N_a}}|\boldsymbol{\Sigma}_i+\boldsymbol{\Sigma}_j|^{-1}},\end{aligned} \tag{17}$$

where it can be shown that we only need to calculate the derivative of $|\boldsymbol{\Sigma}_i+\boldsymbol{\Sigma}_j|$ with respect to $\boldsymbol{H}$ if we would like to figure out the derivative of R_L^M with respect to $\boldsymbol{H}$. Therefore, take $\boldsymbol{\Sigma}_i = \rho\boldsymbol{H}\boldsymbol{V}_i\boldsymbol{H}^H + \boldsymbol{I}_{N_r}$ into $|\boldsymbol{\Sigma}_i+\boldsymbol{\Sigma}_j|$ and the derivative of $|\boldsymbol{\Sigma}_i+\boldsymbol{\Sigma}_j|$ with respect to $\boldsymbol{H}$ can be obtained as:

$$\begin{aligned}\frac{\partial|\boldsymbol{\Sigma}_i+\boldsymbol{\Sigma}_j|}{\partial\boldsymbol{H}} &= \frac{\partial|\rho\boldsymbol{H}\left(\boldsymbol{V}_i+\boldsymbol{V}_j\right)\boldsymbol{H}^H+2\boldsymbol{I}_{N_r}|}{\partial\boldsymbol{H}}\\ &= \frac{\partial|\boldsymbol{H}\left(\boldsymbol{V}_i+\boldsymbol{V}_j\right)\boldsymbol{H}^H|}{\partial\boldsymbol{H}},\end{aligned} \tag{18}$$

where the symbol ∂ is used to denote partial derivative. Besides, the coefficient ρ and the identity matrix $\boldsymbol{I}_{N_r}$ can be neglected as they are constant.

Please note that $\boldsymbol{H}$ is a complex matrix, and hence, the derivative of $|\boldsymbol{\Sigma}_i+\boldsymbol{\Sigma}_j|$ is related to the real part and the imaginary part of $\boldsymbol{H}$. Consequently, the derivative of $|\boldsymbol{\Sigma}_i+\boldsymbol{\Sigma}_j|$ with respect to $\boldsymbol{H}$ is given based on the rule of complex derivative in [74]:

$$\begin{aligned}\frac{\partial|\boldsymbol{\Sigma}_i+\boldsymbol{\Sigma}_j|}{\partial\boldsymbol{H}} &= \left(\frac{\partial|\boldsymbol{H}\left(\boldsymbol{V}_i+\boldsymbol{V}_j\right)\boldsymbol{H}^H|}{2\partial\Re\boldsymbol{H}} - i\frac{\partial|\boldsymbol{H}\left(\boldsymbol{V}_i+\boldsymbol{V}_j\right)\boldsymbol{H}^H|}{2\partial\Im\boldsymbol{H}}\right)\\ &= |\boldsymbol{\Sigma}_i+\boldsymbol{\Sigma}_j|\left[\left(\boldsymbol{V}_i+\boldsymbol{V}_j\right)\boldsymbol{H}^H\left(\boldsymbol{\Sigma}_i+\boldsymbol{\Sigma}_j\right)^{-1}\right]^T,\end{aligned} \tag{19}$$

and the complex conjugate derivative yields:

$$\begin{aligned}\frac{\partial|\boldsymbol{\Sigma}_i+\boldsymbol{\Sigma}_j|}{\partial\boldsymbol{H}^*} &= \left(\frac{\partial|\boldsymbol{H}\left(\boldsymbol{V}_i+\boldsymbol{V}_j\right)\boldsymbol{H}^H|}{2\partial\Re\boldsymbol{H}} + i\frac{\partial|\boldsymbol{H}\left(\boldsymbol{V}_i+\boldsymbol{V}_j\right)\boldsymbol{H}|}{2\partial\Im\boldsymbol{H}}\right)\\ &= |\boldsymbol{\Sigma}_i+\boldsymbol{\Sigma}_j|\left[\left(\boldsymbol{\Sigma}_i+\boldsymbol{\Sigma}_j\right)^{-1}\boldsymbol{H}\left(\boldsymbol{V}_i+\boldsymbol{V}_j\right)\right],\end{aligned} \tag{20}$$

where $\Re$ and $\Im$ refer to the real and imaginary parts. Finally, the derivative of R_L^M with respect to $\boldsymbol{H}$ is given by:

$$\frac{\partial R_L^M}{\partial\boldsymbol{H}} = K_{N_a}^{-1}\sum_{i=1}^{K_{N_a}}\frac{\sum_{j=1}^{K_{N_a}}|\boldsymbol{\Sigma}_i+\boldsymbol{\Sigma}_j|^{-2}\left[\frac{\partial|\boldsymbol{\Sigma}_i+\boldsymbol{\Sigma}_j|}{\partial\boldsymbol{H}}+\frac{\partial|\boldsymbol{\Sigma}_i+\boldsymbol{\Sigma}_j|}{\partial\boldsymbol{H}^*}\right]}{\sum_{j=1}^{K_{N_a}}|\boldsymbol{\Sigma}_i+\boldsymbol{\Sigma}_j|^{-1}}. \tag{21}$$

Afterwards, we can calculate the derivative of $\boldsymbol{H}$ with respect to distance $\boldsymbol{D}$. Firstly, the channel matrix $\boldsymbol{H}$ is in the form of:

$$\boldsymbol{H} = \begin{bmatrix} h_{11} & h_{12} & \cdots & h_{1N_t}\\ h_{21} & h_{22} & \cdots & h_{2N_t}\\ \vdots & \vdots & \vdots & \vdots\\ h_{N_r1} & h_{N_r2} & \cdots & h_{N_rN_t}\end{bmatrix}, \tag{22}$$

and the corresponding distance matrix is given by:

$$\boldsymbol{D} = \begin{bmatrix} d_{11} & d_{12} & \cdots & d_{1N_t} \\ d_{21} & d_{22} & \cdots & d_{2N_t} \\ \vdots & \vdots & \vdots & \vdots \\ d_{N_r1} & d_{N_r2} & \cdots & d_{N_rN_t} \end{bmatrix}, \tag{23}$$

where h_{ij} and d_{ij} represent the channel and the distance from the j^{th} Tx antenna to the i^{th} Rx antenna, respectively, for $i = 1, 2, \ldots, N_r$ and $j = 1, 2, \ldots, N_t$. Hence, the derivative of $\boldsymbol{H}$ with respect to $\boldsymbol{D}$ can be calculated by the point-to-point derivative because only the corresponding d_{ij} of $\boldsymbol{D}$ is related to h_{ij} in $\boldsymbol{H}$ and the derivative of $\boldsymbol{H}$ with respect to $\boldsymbol{D}$ is in the form of:

$$\frac{\partial \boldsymbol{H}}{\partial \boldsymbol{D}} = \begin{bmatrix} \frac{\partial h_{11}}{\partial d_{11}} & \frac{\partial h_{12}}{\partial d_{12}} & \cdots & \frac{\partial h_{1N_t}}{\partial d_{1N_t}} \\ \frac{\partial h_{21}}{\partial d_{21}} & \frac{\partial h_{22}}{\partial d_{22}} & \cdots & \frac{\partial h_{2N_t}}{\partial d_{2N_t}} \\ \vdots & \vdots & \vdots & \vdots \\ \frac{\partial h_{N_r1}}{\partial d_{N_r1}} & \frac{\partial h_{N_r2}}{\partial d_{N_r2}} & \cdots & \frac{\partial h_{N_rN_t}}{\partial d_{N_rN_t}} \end{bmatrix}. \tag{24}$$

Recall that the path loss has to be considered in our A2G communication links. So, the element h_{ij} of $\boldsymbol{H}$ including the path loss can be obtained using (5) and (9), and is given by:

$$h_{ij} = \sqrt{P_r} e^{-j\frac{2\pi}{\lambda} d_{ij}}. \tag{25}$$

Hence, the element $\frac{\partial h_{ij}}{\partial d_{ij}}$ of $\frac{\partial \boldsymbol{H}}{\partial \boldsymbol{D}}$ is calculated by:

$$\frac{\partial h_{ij}}{\partial d_{ij}} = \sqrt{P_r} e^{-j\frac{2\pi}{\lambda} d_{ij}} \left[-\frac{\alpha}{d_{ij}} - j\frac{2\pi}{\lambda} \right], \tag{26}$$

and the complex conjugate derivative yields:

$$\frac{\partial h_{ij}^*}{\partial d_{ij}} = \sqrt{P_r} e^{j\frac{2\pi}{\lambda} d_{ij}} \left[-\frac{\alpha}{d_{ij}} + j\frac{2\pi}{\lambda} \right]. \tag{27}$$

Then, as the height of UAVs is fixed to h_d and each UAV has only one Tx antenna, the coordinate matrix $\boldsymbol{P}_d$ of the UAVs can be represented by:

$$\boldsymbol{P}_d = \begin{bmatrix} P_{d_1} \\ P_{d_2} \\ \vdots \\ P_{d_{N_d}} \end{bmatrix} = \begin{bmatrix} x_{d_1} & y_{d_1} \\ x_{d_2} & y_{d_2} \\ \vdots & \vdots \\ x_{d_{N_d}} & y_{d_{N_d}} \end{bmatrix}. \tag{28}$$

Additionally, the coordinate matrix $\boldsymbol{P}_u$ representing the coordinates of the Rx antennas of the u^{th} GU is given by:

$$\boldsymbol{P}_u = \begin{bmatrix} P_{u_1} \\ P_{u_2} \\ \vdots \\ P_{u_{N_r}} \end{bmatrix} = \begin{bmatrix} x_{u_1} & y_{u_1} \\ x_{u_2} & y_{u_2} \\ \vdots & \vdots \\ x_{u_{N_r}} & y_{u_{N_r}} \end{bmatrix}. \tag{29}$$

Then, the derivative of $\boldsymbol{D}$ with respect to $\boldsymbol{P}_d$ can be calculated by:

$$\frac{\partial \boldsymbol{D}}{\partial \boldsymbol{P}_d} = \begin{bmatrix} \frac{\partial d_{11}}{\partial P_{d_1}} & \frac{\partial d_{11}}{\partial P_{d_2}} & \cdots & \frac{\partial d_{11}}{\partial P_{d_{N_d}}} \\ \frac{\partial d_{21}}{\partial P_{d_1}} & \frac{\partial d_{21}}{\partial P_{d_1}} & \cdots & \frac{\partial d_{21}}{\partial x_{P_{N_d}}} \\ \vdots & \vdots & \vdots & \vdots \\ \frac{\partial d_{N_rN_d}}{\partial P_{d_1}} & \frac{\partial d_{N_rN_d}}{\partial P_{d_1}} & \cdots & \frac{\partial d_{N_rN_d}}{\partial P_{d_{N_d}}} \end{bmatrix}, \tag{30}$$

while the element $\frac{\partial d_{ij}}{P_{d_{n_d}}}$ for $n_d = 1, 2, \ldots, N_d$ is calculated based on (4), and can be expressed by:

$$\begin{aligned} \frac{\partial d_{ij}}{P_{d_{n_d}}} &= \frac{\begin{bmatrix} x_{d_{n_d}} - x_{u_{n_r}} & y_{d_{n_d}} - y_{u_{n_r}} \end{bmatrix}}{\sqrt{(x_{d_{n_d}} - x_{u_{n_r}})^2 + (y_{d_{n_d}} - y_{u_{n_r}})^2 + h^2}} \\ &= \begin{bmatrix} \frac{x_{d_{n_d}} - x_{u_{n_r}}}{d_{ij}} & \frac{y_{d_{n_d}} - y_{u_{n_r}}}{d_{ij}} \end{bmatrix}. \end{aligned} \tag{31}$$

Consequently, the derivative is in the form of:

$$\frac{\partial \boldsymbol{D}}{\partial \boldsymbol{P}_d} = \begin{bmatrix} \frac{\partial d_{11}}{\partial x_{d_1}} & \frac{\partial d_{11}}{\partial y_{d_1}} & \cdots & \frac{\partial d_{11}}{\partial x_{d_{N_d}}} & \frac{\partial d_{11}}{\partial y_{d_{N_d}}} \\ \frac{\partial d_{21}}{\partial x_{d_1}} & \frac{\partial d_{21}}{\partial y_{d_1}} & \cdots & \frac{\partial d_{21}}{\partial x_{d_{N_d}}} & \frac{\partial d_{21}}{\partial y_{d_{N_d}}} \\ \vdots & \vdots & \vdots & \vdots & \vdots \\ \frac{\partial d_{N_rN_d}}{\partial x_{d_1}} & \frac{\partial d_{N_rN_d}}{\partial y_{d_1}} & \cdots & \frac{\partial d_{N_rN_d}}{\partial x_{d_{N_d}}} & \frac{\partial d_{N_rN_d}}{\partial y_{d_{N_d}}} \end{bmatrix}. \tag{32}$$

Finally, the derivative of R_L^M with respect to the location of the UAVs $\boldsymbol{P}_d$ can be obtained as:

$$\frac{\partial R_L^M}{\partial \boldsymbol{H}} \cdot \frac{\partial \boldsymbol{H}}{\partial \boldsymbol{D}} \cdot \frac{\partial \boldsymbol{D}}{\partial \boldsymbol{P}_d} = \frac{\partial R_L^M}{\partial \boldsymbol{P}_d}. \tag{33}$$

Hence, since the gradient of R_L^M of the GUs can be obtained and the locations of each UAV will be periodically updated through A2A links, the UAVs can use the gradient descent algorithm to find the position that can maximize the sum rate of all GUs. The whole procedure is summarized in Algorithm 1.

Algorithm 1 Deployment procedure of IM-UAV communication system.

1: **for** n from 1 to N_u **do**
2: Obtain the lower bound of achievable rate R_L^M
3: Take the derivative of R_L^M with respect to channel $\boldsymbol{H}$ using (21)
4: Take the derivative of $\boldsymbol{H}$ with respect to $\boldsymbol{D}$ according to (24)
5: Take the derivative of $\boldsymbol{D}$ with respect to $\boldsymbol{P}_d$ as in (32)
6: Obtain the derivative of R_L^M with respect to the location of UAVs $\boldsymbol{P}_d$ through chain rule using (33)
7: **end for**
8: Add the gradients of all N_u GUs together to get the final gradient
9: Apply gradient descent algorithm and deploy UAVs to the position when converging

C. Energy Consumption Model of Communication

The performance of UAV communication system is fundamentally limited by the on-board energy. The on-board energy is mainly consumed by two parts, one is used for flying, while the other is used to establish communication. The major task of this work is about the A2G communications between the UAVs and the GUs. Therefore, it is important to design an energy-efficient UAV communication scheme to reduce the energy consumed per information bit. The calculation of all energy consumed by data transmission in the UAV-assisted communication system is quite different from that in

traditional communication system especially in our proposed IM-UAV communication system, since all UAVs in our IM-UAV communication system will be active all the time. For simplicity, the baseband signal processing blocks (e.g., source coding, pulse shaping and digital modulation) have been omitted [75]. Given the UAV is a power limited platform, we care more about the communication energy consumed at the Tx side (UAV) than the Rx side, and hence the energy consumption at the Rx side will not be considered in this paper.

The total average power consumption along the signal path is composed by two main components [76]: the power consumption of the power amplifier P_a and other circuit blocks P_c. The first term P_a depends on the transmission power P_t and the power consumption of the power amplifier can be calculated by [77]:

$$P_a = \frac{P_t}{\eta}, \tag{34}$$

where η is the drain efficiency, which we set as 10% in our system as OFDMA is employed to support multi-user communication [78]. The second term P_c is composed by [79]:

$$P_c = P_{\text{DAC}} + P_{\text{Mix}} + P_{\text{Filt}} + P_{\text{Syn}}, \tag{35}$$

where P_{DAC}, P_{Mix}, P_{Filt} and P_{Syn} are the power consumption values for the digital-to-analogue converter (DAC), the mixer, the filter and the frequency synthesizer. Finally, according to the power constraint in (11), the total power consumed by the UAVs can be written as:

$$P_{\text{sum}} = N_a P_a + N_d P_c. \tag{36}$$

A binary-weighted current-steering DAC is considered in our system [80] and the power consumption of the DAC consists of two components: static power consumption P_s and dynamic power consumption P_d. Firstly, the total output current I_o of a N-bit DAC is closely related to the unit current source, which is denoted by I_u. For the i^{th} bit, totally 2^i unit current resources are needed. Thus, the total number of I_u, which is also known as code k, can be expressed by:

$$k = \sum_{i=0}^{N-1} 2^i b_i, \tag{37}$$

where b_i is independent binary random variables taking values of 0 or 1 with percentage of 50%. Here, b_{N-1} is the most significant bit and b_0 is the least significant bit. Therefore, the total output current is given by:

$$I_o = k I_u. \tag{38}$$

Consequently, the static power consumption can be calculated by:

$$P_s = V_{\text{dd}} E\left[I_o\right] = \frac{1}{2} V_{\text{dd}} I_u \left(2^N - 1\right), \tag{39}$$

where V_{dd} is the power supply voltage.

The dynamic power consumption occurs during the switching process (on or off) between symbols. For simplicity, we assume that each switch has the same parasitic capacitance C_p and each switch has a chance of 50% to change status during a transition. Then, the average value of P_d can be obtained by $P_d = \frac{NC_p f_s V_{\text{dd}}^2}{2}$ for the first-order approximation [81]. The sampling frequency can be approximately taken as $f_s = 2(2B + f_{\text{cor}})$ in our proposed system as we assume it is a low intermediate frequency structure, where f_{cor} is the corner frequency of the $\frac{1}{f}$ noise [77] and B is the bandwidth. Thus, the expression for P_d can be rewritten as:

$$P_d = NC_p \left(2B + f_{\text{cor}}\right) V_{\text{dd}}^2. \tag{40}$$

Hence, the total power consumption of the DAC is given by:

$$P_{\text{DAC}} = \beta \left(P_s + P_d\right), \tag{41}$$

where β is a correcting factor to incorporate second-order effects. Hence, we are able to calculate the energy consumed by communication, which can be utilised to analyze EE in the following section.

D. Low-Complexity Detection

For our IM-UAV communication system, the optimal ML detection, which jointly searches all the possible transmit antenna combinations and the modulated symbols, increases exponentially in complexity with the number of UAVs and modulation levels. By contrast, both the maximal-ratio combining and the zero-forcing algorithms have very low-complexity, but their error performance is significantly worse than the ML. In order to reduce the computational complexity but also keep the BER performance satisfactory, we propose a new low-complexity detection scheme that can provide a trade-off between BER performance and complexity. The proposed low-complexity detection scheme utilizes the fact that the signals transmitted from different UAVs have different signal power at the receiver side, which typically exists in UAV-assisted communication networks, to identify signals received from different UAVs. Besides, by additionally considering the phase difference of the data symbols, the detection accuracy can be further improved.

We assume perfect channel knowledge at the GUs and that the GUs are aware of the number of activated UAVs N_a. Therefore, all possible combinations of the channels can be represented by the set:

$$\mathcal{H} = \{\boldsymbol{h}_1, \boldsymbol{h}_2, \ldots, \boldsymbol{h}_{n_h}, \ldots, \boldsymbol{h}_{N_h}\}, \tag{42}$$

where N_h is the number of all channel combinations and can be calculated by:

$$N_h = \left\lfloor \log_2 \binom{N_a}{N_d} \right\rfloor, \tag{43}$$

where N_d it the total number of UAVs, $\lfloor \cdot \rfloor$ is the floor operation and $\binom{\cdot}{\cdot}$ stands for the binomial coefficient. For example, if we have 4 UAVs and only 3 of them are activated, the $N_h = 4$ possible combinations of the channels is shown in Table I, where $\boldsymbol{h}_i$ indicates the i^{th} possible combination and h_i indicates the channel of the i^{th} UAV, for $i = 1, 2, 3, 4$.

After the FFT operation at the receiver side, all the N_h possible combinations of the transmitted signals $\hat{\boldsymbol{x}} =$

TABLE I: Example for $N_d = 4$ and $N_a = 3$.

Combinations	Corresponding block
$\boldsymbol{h}_1$	$\{h_1, h_2, h_3\}$
$\boldsymbol{h}_2$	$\{h_2, h_3, h_4\}$
$\boldsymbol{h}_3$	$\{h_1, h_2, h_4\}$
$\boldsymbol{h}_4$	$\{h_1, h_3, h_4\}$

$[\boldsymbol{x}_1, \boldsymbol{x}_2, \ldots, \boldsymbol{x}_{n_h}, \ldots, \boldsymbol{x}_{N_h}]$ in frequency domain can be obtained by:

$$\boldsymbol{x}_{n_h} = \boldsymbol{h}_{n_h}^{\dagger} \boldsymbol{y}, \tag{44}$$

$$= \boldsymbol{x} + \boldsymbol{h}_{n_h}^{\dagger} \boldsymbol{n}, \tag{45}$$

$$= [S_1, S_2, \ldots, S_{n_a}, \ldots, S_{N_a}]^T, \tag{46}$$

where $(\cdot)^{\dagger}$ indicates the pseudo inverse operation and $(\cdot)^T$ denotes the transpose. Here, the n_h^{th} possible recovered signal $\boldsymbol{x}_{n_h}$ has a size of N_a and S_{n_a} represents the n_a^{th} data symbol of $\boldsymbol{x}_{n_h}$. Then, the Euclidean distances between the constellation symbols and each possible received data symbol S_{n_a} can be calculated based on the cosine rule in (47). Therefore, a Euclidean distance vector $\boldsymbol{D}_s = [d_1, d_2, \ldots, d_{n_h}, \ldots, d_{N_h}]$ can be obtained by calculating all N_h possible combinations in $\hat{\boldsymbol{x}}$, where d_{n_h} is the sum Euclidean distance of all symbols from n_h^{th} combination $\boldsymbol{x}_{n_h}$. Thereafter, based on the sum Euclidean distances that has been obtained, the combinations that has the smallest distance will be considered as the original transmitted data symbol vector.

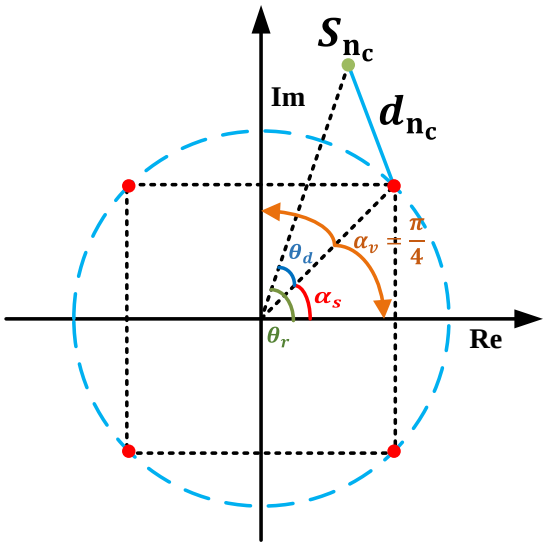

Fig. 5: Illustration of calculating smallest distance with QPSK by amplitude-phase detection.

According to the cosine rule, it states that the third side of a triangle can be obtained when two sides and their enclosed angle are known, which can be evaluated as:

$$g^2 = a^2 + b^2 - 2ab\cos\gamma. \tag{47}$$

Therefore, it could be shown that the length of g is only related to the angle γ, when a and b are fixed. For simplicity, we assume that the modulation scheme used in the system is star-QAM or M-PSK, which keeps all constellation symbols around a ring with fixed amplitudes but different phases. However, if there is a need to use other modulation scheme that is not naturally grouped by amplitudes and phases, it is necessary to "manually" cluster constellation symbols into different groups according to the level of amplitudes. For example, 16-QAM whose constellation symbols form a "square", the detector then has to cluster those symbols into different groups according to their amplitudes and phases. Since cosine is monotonically decreasing in the range $[0, \pi]$, the smallest Euclidean distance between S_{n_a} and the potential constellation symbols can be obtained when the smallest phase difference is achieved. Hence, we name this detection scheme amplitude-phase detection. To further illustrate, let us consider a QPSK modulated system as shown in Fig. 5. In this example, the modulus of the received data symbol S_{n_c} and the modulus of the constellation symbols are known and fixed, and our target is to find the smallest phase difference between S_{n_c} and the constellation symbols. The solution to identify which range the received symbol belongs to is summarized in Algorithm 2.

Algorithm 2 Operating procedure of minimum phase difference.

1: Obtain the phase θ_r of the received symbol
2: Obtain the start phase α_s of the constellation symbols
3: **if** α_s = 0 **then**
4: $\quad F = \frac{\lfloor \theta_r - \alpha_v \rfloor}{\alpha_v} \mod 2$
5: **else**
6: $\quad F = \frac{\lfloor \theta_r \rfloor}{\alpha_v} \mod 2$
7: **end if**
8: $\theta_d = |F \times \alpha_v - (\theta_r \mod \alpha_v)|$

As shown in Fig. 5, the detector obtains the phase θ_r of the received symbol and the start phase α_s of the constellation symbols, where the start phase α_s means the smallest angle of constellation symbols in range $[0, 2\pi]$ and $\alpha_s = \frac{\pi}{4}$ in this case. Then, we do the parity check based on the value of α_s and the valid phase range α_v, where α_v indicates the valid phase range of constellation symbols around the same ring, which can be calculated by $\alpha_v = \frac{\pi}{M}$, where M is the modulation order. To further illustrate, we consider the top right constellation symbol on the ring of QPSK in Fig. 5 as an example. Here, it could be found that when S_{n_c} is located within the phase range of $(0, \frac{\pi}{2})$, the phase difference will be calculated based on this constellation symbol. However, if S_{n_c} is located outside this range, it will choose other constellation symbol as a base to calculate the phase difference. Therefore, it can be seen that the valid phase range is $\frac{\pi}{4}$ on both side of this constellation symbol. Since all constellation symbols around the same ring are space arranged with equal phase difference, the valid phase range is identical for all constellation symbols around the same ring. Finally, the smallest phase difference θ_d between the received symbol and the constellation symbols is related to multiple of α_v, and thus a flag F is set to identify the parity of $\lfloor \theta_r \rfloor$ or $\lfloor \theta_r - \alpha_v \rfloor$. Now, the smallest distance can also be calculated based on θ_d and the cosine formula presented in (47).

TABLE II: Simulation parameters

Parameter	Symbol	Value	Parameter	Symbol	Value
K-factor	K	3	Bandwidth	B	40 MHz
Noise PSD	N_0	-174 dBm/Hz	Transmission power	P_t	$1 \sim 40$ dBm
Carrier frequency	f_c	5.8 GHz	Path loss exponent	α	2
UAV height	h_d	100 m	Speed of light	c	3×10^8 m/s
Number of UAVs	N_d	4	Number of activated UAVs	N_a	$1 \sim 4$
Number of Rx antennas	N_r	4	Number of subcarriers	N_s	512
Number of data subcarriers	N_{ds}	468	Learning rate	l_r	5
Number of GUs	N_u	18	Number of epochs	N_e	300
Correcting factor	β	1	Drain efficiency	η	10%
Power supply	V_{dd}	3 V	Resolution of DAC	N	10 bits
Unit current source	I_u	10 μ A	Parasitic capacitance	C_p	1 pF
Corner frequency	f_{cor}	1 MHz	Power consumption of filter	P_{filt}	2.5 mW
Power consumption of synthesizer	P_{syn}	50 mW	Power consumption of mixer	P_{mix}	30.3 mW

Afterwards, all those smallest distances of the received symbols will be added together for each combination and the combination that results in the smallest $\boldsymbol{d}_{n_c}$ will be considered as the detected symbols. Therefore, the index of the activated UAVs can be obtained according to this combination. Finally, we use the corresponding channel combination to do the data bits recovery with ML detection. Our proposed low-complexity detection scheme separately detects the index symbols and data symbols, which largely reduce the complexity of the optimal ML detection. For example, we consider one scenario that $N_a = 2$ UAVs will be activated and totally I possible combinations of index bits (activated UAV) is considered. Then, if S constellation symbols and T rings are assumed, the search space for the ML detection scheme is $I \times S^{N_a}$, while the search space of the proposed low-complexity detection scheme is $I \times T + S^{N_a}$. Therefore, the search space of our proposed low-complexity detection scheme is significantly smaller than that of ML detection scheme as discussed numerically in the following section.

III. Simulation Results

In this section, we investigate the performance of our proposed IM-UAV communication system in a 1 km $\times$ 1 km square area with $N_u = 18$ GUs and $N_d = 4$ UAVs. For all GUs in this target area, we assume that $N_r = 4$ antennas are mounted on their equipments. UAVs operate at a height of $h_d = 100$ m and each is equipped with one antenna. Then, we set the carrier frequency to $f_c = 5.8$ GHz for the A2G communication, while the path loss exponent α and the Rician K-factor K are set to 2 and 3, respectively. Meanwhile, the noise power spectral density (PSD) N_0 is set to -174 dBm/Hz and the transmission power P_t of the UAVs is in the range from 1 dBm to 40 dBm. Additionally, OFDMA is employed to support multi-user communications, where the total bandwidth B allocated to all GUs is 40 MHz. In our system, the whole bandwidth is divided into 512 subcarriers and only 468 of them will be used as data subcarriers to transmit data bits, while the rest will be set as guard intervals [82]. Besides, all GUs in our system has the same weight, which means 26 subcarriers will be assigned to each user. Moreover, we assume the UAVs are able to obtain the locations of GUs and that the UAV's speed is much faster than that of GUs, which means the UAVs can always catch the steps of GUs. Therefore, the distribution of GUs in each time slot can be considered as a snapshot to the UAVs, which means they can approximately be treated as fixed[2] in each time slot.

On the other hand, in the research reviewed in Section I.B concerning the the energy consumption of UAVs, the propulsion energy is mainly considered for the path planning of the UAV movement. In those trajectory-related work, single UAV or fixed-wing UAVs has been considered to serve static GUs, where the UAV needs to move from one location to another and path planning can be optimized for improved propulsion energy efficiency. Here, the propulsion energy has been considered as the main energy consumption factor, while communications energy consumption has been ignored. However, in our proposed work we aim to find the optimal UAV locations to serve the GUs and we do not focus on the path plan for the UAVs to move from the initial location to the destination. Hence, we focus on the communications energy consumption, while the propulsion energy consumption would be similar to the analysis presented in the previous research about path planning.

In this work, all simulations are run on MATLAB 2022b and the detailed simulation parameters are listed in Table II. We perform the Monte Carlo simulation based on different distributions of N_u GUs in a 1 km $\times$ 1 km target area by uniformly generating the coordinates of the GUs. For simplicity, only one snapshot (a random distribution of GUs) is taken to illustrate the deployment process of UAVs in our proposed IM-UAV communication system as different distributions of GUs offer similar "trends". Furthermore, the EE of the proposed IM-UAV communication system and the BER performance of low-complexity detection scheme are obtained from Monte Carlo Simulation by testing millions of GUs' distributions. Here, it is worth noting that $\boldsymbol{H}_{\text{LoS}}$ is only used to optimize the deployment locations of UAVs in our proposed IM-UAV communication system, while the other simulations are based on the complete Rician channel with

[2] If the UAV speed is slower than that of the GUs, then, the GUs cannot be considered as fixed points in this case and the gradient will rapidly change during the deployment process.

both LoS and NLoS components. In the following, we analyze the effect of the UAV deployment on the average rate of all GUs. Afterwards, the EE of the proposed IM-UAV system will be investigated. Finally, the BER performance of our proposed low-complexity detection scheme will be examined.

A. UAV Deployment

In our proposed IM-UAV communication system, the sum rate of all GUs is taken as the objective function for optimizing the deployment of UAVs. Fig. 6 depicts the performance of our proposed deployment schemes in the scenario of 2 activated UAVs out of 4 deployed UAVs. Based on the gradient of the rate in (33) with respect to the position of all UAVs, it can be found from Fig. 6(a) that the average downlink rate of all GUs in the target area steadily increases by the gradient descent algorithm. Finally, the curves of Fig. 6(a) reach steady state after enough number of epochs, where the epoch is the maximum number of steps the algorithm will run for convergence. The blue curve in Fig. 6(a), which represents the lower bound of the achievable rate, is obtained from (16), while the red curve named by 'Real Rate' is obtained from (8) and (14) of [83] to indicate the true rate of the GUs by Cholesky decomposition [84]. It can be seen from Fig. 6(a) that the trend of the lower bound and the real rate is consistent and this means the deployment of multiple UAVs does effectively improve the QoS of the downlink rate.

In this simulation, the locations of GUs are randomly generated in the target area and the purpose of this simulation is to take one snapshot of GU distribution as an example to illustrate the deployment process of UAVs. The purpose of this simulation is also to show how the deployment (mobility) of UAVs improves the communication quality when comparing with those fixed BSs without any mobility. In other words, the downlink rate of GUs cannot be adaptively adjusted if the BSs are fixed rather than fly BSs with mobility. Therefore, we consider those hollow red circles in Fig. 6(b) as the benchmark to represent fixed BSs without mobility. Fig. 6(b) shows the distribution of GUs and the locations of UAVs in correspondence with this two curves that have been depicted in Fig. 6(a). Again, it is worth noting that the value of average downlink rate illustrated in Fig. 6(a) is only corresponding to this specific distribution scenario presented by Fig. 6(b). Here, all UAVs are represented by red circles and GUs are indicated by blue crosses. The hollow red circles is the initial location of UAVs (UAV_I), and the solid ones are the final location (UAV_F) where UAVs will be deployed.

B. Energy-Efficiency of IM-UAV Communication

Unlike the simulation of UAV deployment that only takes one snapshot of GU distribution as an example, we run a Monte Carlo simulation based on millions of different GU distributions in the target area for the purpose of generality. For each snapshot of GU distribution, one simulation result will be obtained. Therefore, the simulation results illustrated by Fig. 7 are the mean values of all those snapshots at different transmission power.

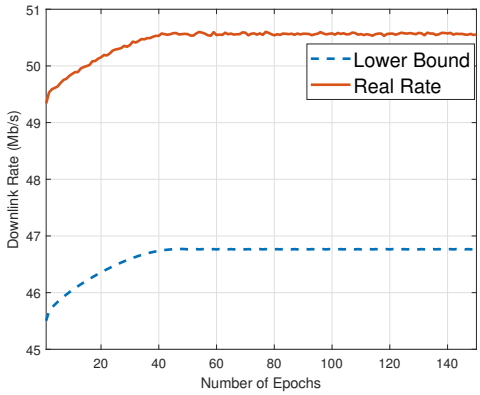

(a) The trend of average downlink rate of the GUs during the UAV deployment process.

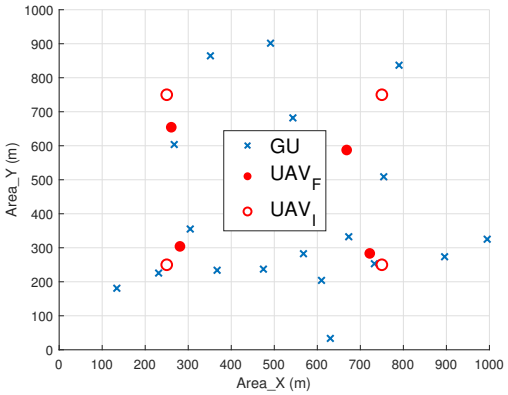

(b) The location of UAVs before and after the deployment process, where UAV_I and UAV_F indicate the initial locations and the final locations, respectively.

Fig. 6: The deployment process of 2 activated UAVs out of 4 deployed UAVs with 18 GUs within a 1 km $\times$ 1 km target area by gradient descent algorithm in the proposed IM-UAV communication system.

In Fig. 7(a), we show the average capacity of GUs with different activated patterns, where we show 4 curves that represent different activated patterns. Here, the legend "x-UAV" means only x UAVs has been activated among all 4 deployed UAVs. Note that the benchmark scheme in this case is the "4-UAV" scenario, which indicates the scenario of fully activated UAVs, where no IM has been employed. With the increase of transmission power, it can be seen that the capacity will increase. Besides, increasing the number of activated UAVs improves the achievable capacity, as shown in Fig. 7(a). However, it also can be deduced that the capacity at the level of high transmission power increases slowly, which means the overall increase of information bits is smaller than the increase of the transmission power.

This phenomenon is also reflected by Fig. 7(b), where at lower levels of transmission power, the EE of "4-UAV" is the best as it transmits the most information bits with the same transmission power. However, with the increase of transmission power, the trend of all curves increases to a peak and then starts to reduce. Besides, it can be found that the EE

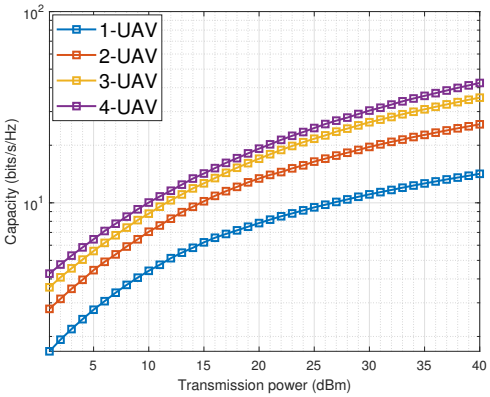

(a) Average capacity of different activated patterns.

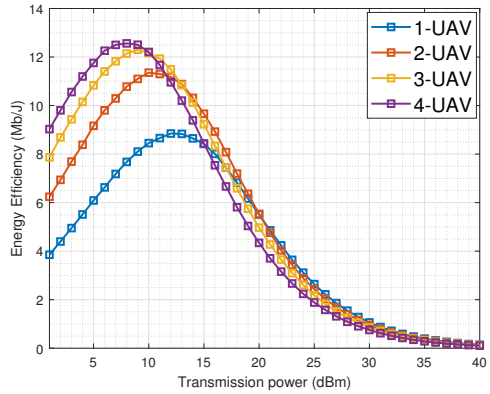

(b) Energy-efficiency of different activated patterns.

Fig. 7: Average capacity and energy-efficiency of different activated patterns in the proposed IM-UAV communication system with 4 UAVs and 18 GUs at different transmission power within a 1 km $\times$ 1 km target area.

of IM-UAV communication starts to surpass the fully-activated scenario at around 15 dBm transmission power, which is the practical transmission power to consider. Explicitly, the transmission power of common UAVs will not operate in the 5 dBm to 20 dBm range due to the relatively high A2G path loss, where Fig. 8 also indicates that the BER performance of the system is bad in this range. Hence, it can be concluded that the IM-UAV system attains a higher EE compared to activating all UAVs, in the practical transmission power range as depicted in Fig. 7(b).

C. Performance of Low-complexity Detection

Fig. 8 shows the BER performance of the proposed low-complexity detection by considering 8-PSK modulation scheme. Here, the optimal ML detection is considered as the benchmark to illustrate the performance of the proposed low-complexity detection scheme. In this case, we test three activation patterns that activates 1 UAV, 2 UAVs and 3 UAVs, when 4 UAVs are deployed. Below a transmission power of 27 dBm, the low-complexity and ML detection follow the same pattern, where activating more UAVs results in a worse BER performance. However, the performance of 2 activated UAVs and 3 activated UAVs becomes better than that of 1 activated UAV scenario with the increase of the transmission power for the proposed low-complexity detection scheme. This is caused by the characteristics of our proposed detection scheme as we consider both the amplitude and phase of the received signals. In the low transmission power range, the signal is deeply affected by the noise, where activating more UAVs results in a higher transmission rate, which results in more detection errors due to the noise. On the other hand, this phenomenon will be improved with the increase of transmission power because the average path loss of 2 activated UAV and 3 activated UAV is smaller than that of 1 activated UAV scenario and noise is not the dominant factor that affects the BER performance in the higher transmit power scenarios.

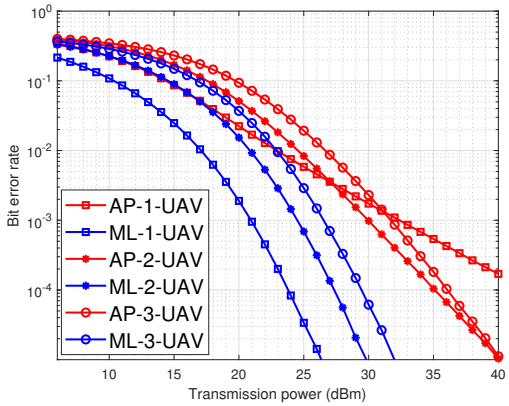

Fig. 8: BER performance of low-complexity detection and ML detection by 8-PSK in the proposed IM-UAV communication system with 4 UAVs and 18 GUs.

Based on the BER comparison between two detection schemes, it can be seen that the degradation of BER performance is mainly caused by the index detection. In our proposed low-complexity detection scheme, we firstly detect the index of activated UAVs by analyzing the amplitude and phase of the constellation symbols. As mentioned before, the complexity of this scheme depends on the level of amplitudes (number of rings) and the corresponding phase differences of constellation symbols around these rings. Therefore, instead of searching all possible combinations of index symbols and data symbols, this amplitude-phase detection scheme will reduce the detection complexity significantly when high order modulation schemes or large number of UAVs is employed. In Table III, a scenario with $N_a = 3$ out of 4 UAVs activated has been included to illustrate the complexity of this two detection schemes. It can be found that totally $I = 4$ combinations of index bits or activated UAVs exist, therefore, according to the number of constellation symbols S and the number of rings T for each modulation scheme, the search space can be obtained. However, the reduction of complexity also cause a degradation in the BER performance, because the wrong detection of index symbols causes severe effects on the following detection of data symbols. Therefore, it is a complexity-performance trade-off.

TABLE III: Search space for $N_d = 4$ and $N_a = 3$ by QPSK, 8-PSK and star 16-QAM.

Modulation	ML detection	Low-complexity detection
QPSK	256	68
8-PSK	2048	516
Star 16-QAM	16384	4104

IV. Conclusion

In this work, we proposed an IM based UAV wireless communication system, which aims to increase the EE of power-limited UAV platforms. Furthermore, by combining the UAV communication system with IM, the BER performance of the system could be improved. Besides, based on the proposed IM-UAV communication system, a multi-UAV deployment scheme has been designed to maximize the downlink sum rate of all GUs. Additionally, we designed a low-complexity detection scheme to separately detect the index symbols and the data symbols, rather than jointly detecting them using the exhaustive search in the IM-UAV scheme.

References

[1] R. Gupta, A. Nair, S. Tanwar, and N. Kumar, "Blockchain-assisted secure UAV communication in 6G environment: Architecture, opportunities, and challenges," *IET communications*, vol. 15, no. 10, pp. 1352–1367, 2021.

[2] X. Jiang, M. Sheng, Z. Nan, X. Chengwen, L. Weidang, and W. Xianbin, "Green UAV communications for 6G: A survey," *Chinese Journal of Aeronautics*, vol. 35, no. 9, pp. 19–34, 2022.

[3] Z. Yuan, J. Jin, L. Sun, K.-W. Chin, and G.-M. Muntean, "Ultra-reliable IoT communications with UAVs: A swarm use case," *IEEE Communications Magazine*, vol. 56, no. 12, pp. 90–96, 2018.

[4] R. Li, X. Li, J. Xu, F. Jiang, Z. Jia, D. Shao, L. Pan, and X. Liu, "Energy-aware decision-making for dynamic task migration in MEC-based unmanned aerial vehicle delivery system," *Concurrency and Computation: Practice and Experience*, vol. 33, no. 22, p. e6092, 2021.

[5] N. Delavarpour, C. Koparan, J. Nowatzki, S. Bajwa, and X. Sun, "A technical study on UAV characteristics for precision agriculture applications and associated practical challenges," *Remote Sensing*, vol. 13, no. 6, p. 1204, 2021.

[6] S. Granados-Bolaños, A. Quesada-Román, and G. E. Alvarado, "Low-cost UAV applications in dynamic tropical volcanic landforms," *Journal of Volcanology and Geothermal Research*, vol. 410, p. 107143, 2021.

[7] F. Ahmed, J. Mohanta, A. Keshari, and P. S. Yadav, "Recent Advances in Unmanned Aerial Vehicles: A Review," *Arabian Journal for Science and Engineering*, vol. 47, no. 7, pp. 7963–7984, 2022.

[8] B. Alzahrani, O. S. Oubbati, A. Barnawi, M. Atiquzzaman, and D. Alghazzawi, "UAV assistance paradigm: State-of-the-art in applications and challenges," *Journal of Network and Computer Applications*, vol. 166, p. 102706, 2020.

[9] A. L. Yingst and V. Marojevic, "Tethered UAV with high gain antenna for BVLOS CNPC: A practical design for widespread use," in *2021 IEEE 22nd International Symposium on a World of Wireless, Mobile and Multimedia Networks (WoWMoM)*. IEEE, 2021, pp. 323–328.

[10] A. Baltaci, M. Klügel, F. Geyer, S. Duhovnikov, V. Bajpai, J. Ott, and D. Schupke, "Experimental UAV data traffic modeling and network performance analysis," in *IEEE INFOCOM 2021-IEEE Conference on Computer Communications*. IEEE, 2021, pp. 1–10.

[11] Y. Zeng, Q. Wu, and R. Zhang, "Accessing from the sky: A tutorial on UAV communications for 5G and beyond," *Proceedings of the IEEE*, vol. 107, no. 12, pp. 2327–2375, 2019.

[12] R. Shahzadi, M. Ali, H. Z. Khan, and M. Naeem, "UAV assisted 5G and beyond wireless networks: A survey," *Journal of Network and Computer Applications*, vol. 189, p. 103114, 2021.

[13] H. Nawaz, H. M. Ali, and A. A. Laghari, "UAV communication networks issues: a review," *Archives of Computational Methods in Engineering*, vol. 28, pp. 1349–1369, 2021.

[14] X. Xu, L. Duan, and M. Li, "UAV placement games for optimal wireless service provision," in *WiOpt*, 2018, pp. 1–8.

[15] X. Wang and L. Duan, "Dynamic pricing and capacity allocation of UAV-provided mobile services," in *IEEE INFOCOM 2019-IEEE Conference on Computer Communications*. IEEE, 2019, pp. 1855–1863.

[16] S. Fu, Y. Tang, N. Zhang, L. Zhao, S. Wu, and X. Jian, "Joint unmanned aerial vehicle (UAV) deployment and power control for Internet of Things networks," *IEEE Transactions on Vehicular Technology*, vol. 69, no. 4, pp. 4367–4378, 2020.

[17] Z. Kaleem, W. Khalid, A. Muqaibel, A. A. Nasir, C. Yuen, and G. K. Karagiannidis, "Learning-aided UAV 3D placement and power allocation for sum-capacity enhancement under varying altitudes," *IEEE Communications Letters*, vol. 26, no. 7, pp. 1633–1637, 2022.

[18] J. Luo, J. Song, F.-C. Zheng, L. Gao, and T. Wang, "User-centric UAV deployment and content placement in cache-enabled multi-UAV networks," *IEEE Transactions on Vehicular Technology*, vol. 71, no. 5, pp. 5656–5660, 2022.

[19] Z. Wang, L. Duan, and R. Zhang, "Adaptive deployment for UAV-aided communication networks," *IEEE transactions on wireless communications*, vol. 18, no. 9, pp. 4531–4543, 2019.

[20] M. H. M. Ghazali, K. Teoh, and W. Rahiman, "A systematic review of real-time deployments of UAV-based LoRa communication network," *IEEE Access*, vol. 9, pp. 124 817–124 830, 2021.

[21] Z. Wang and L. Duan, "Chase or wait: dynamic UAV deployment to learn and catch time-varying user activities," *IEEE Transactions on Mobile Computing*, 2021.

[22] I. Valiulahi and C. Masouros, "Multi-UAV deployment for throughput maximization in the presence of co-channel interference," *IEEE Internet of Things Journal*, vol. 8, no. 5, pp. 3605–3618, 2020.

[23] Y. Wang, M. Chen, Z. Yang, T. Luo, and W. Saad, "Deep learning for optimal deployment of UAVs with visible light communications," *IEEE Transactions on Wireless Communications*, vol. 19, no. 11, pp. 7049–7063, 2020.

[24] G. Wu, W. Jia, and J. Zhao, "Dynamic deployment of multi-UAV base stations with deep reinforcement learning," *Electronics Letters*, 2021.

[25] X. Tang, N. Liu, R. Zhang, and Z. Han, "Deep learning-assisted secure UAV-relaying networks with channel uncertainties," *IEEE Transactions on Vehicular Technology*, vol. 71, no. 5, pp. 5048–5059, 2022.

[26] P. Beigi, M. S. Rajabi, and S. Aghakhani, "An Overview of Drone Energy Consumption Factors and Models," *arXiv preprint arXiv:2206.10775*, 2022.

[27] M. Mozaffari, W. Saad, M. Bennis, and M. Debbah, "Optimal transport theory for power-efficient deployment of unmanned aerial vehicle," in *2016 IEEE international conference on communications (ICC)*. IEEE, 2016, pp. 1–6.

[28] Y. Zeng and R. Zhang, "Energy-efficient UAV communication with trajectory optimization," *IEEE Transactions on Wireless Communications*, vol. 16, no. 6, pp. 3747–3760, 2017.

[29] M. Hua, Y. Wang, Z. Zhang, C. Li, Y. Huang, and L. Yang, "Power-efficient communication in UAV-aided wireless sensor networks," *IEEE Communications Letters*, vol. 22, no. 6, pp. 1264–1267, 2018.

[30] L. Ruan, J. Wang, J. Chen, Y. Xu, Y. Yang, H. Jiang, Y. Zhang, and Y. Xu, "Energy-efficient multi-UAV coverage deployment in UAV networks: A game-theoretic framework," *China Communications*, vol. 15, no. 10, pp. 194–209, 2018.

[31] Y. Zeng, J. Xu, and R. Zhang, "Energy minimization for wireless communication with rotary-wing UAV," *IEEE Transactions on Wireless Communications*, vol. 18, no. 4, pp. 2329–2345, 2019.

[32] H. Yan, Y. Chen, and S.-H. Yang, "New energy consumption model for rotary-wing UAV propulsion," *IEEE Wireless Communications Letters*, vol. 10, no. 9, pp. 2009–2012, 2021.

[33] F. Wu, D. Yang, L. Xiao, and L. Cuthbert, "Energy consumption and completion time tradeoff in rotary-wing UAV enabled WPCN," *IEEE Access*, vol. 7, pp. 79 617–79 635, 2019.

[34] B. Zhu, E. Bedeer, H. H. Nguyen, R. Barton, and J. Henry, "UAV trajectory planning in wireless sensor networks for energy consumption minimization by deep reinforcement learning," *IEEE Transactions on Vehicular Technology*, vol. 70, no. 9, pp. 9540–9554, 2021.

[35] J. Chakareski, S. Naqvi, N. Mastronarde, J. Xu, F. Afghah, and A. Razi, "An energy efficient framework for UAV-assisted millimeter wave 5G heterogeneous cellular networks," *IEEE Transactions on Green Communications and Networking*, vol. 3, no. 1, pp. 37–44, 2019.

[36] J. Ji, K. Zhu, C. Yi, and D. Niyato, "Energy consumption minimization in UAV-assisted mobile-edge computing systems: Joint resource allocation and trajectory design," *IEEE Internet of Things Journal*, vol. 8, no. 10, pp. 8570–8584, 2020.

[37] S. AlJubayrin, F. N. Al-Wesabi, H. Alsolai, M. A. Duhayyim, M. K. Nour, W. U. Khan, A. Mahmood, K. Rabie, and T. Shongwe, "Energy

Efficient Transmission Design for NOMA Backscatter-Aided UAV Networks with Imperfect CSI," *Drones*, vol. 6, no. 8, p. 190, 2022.

[38] S. D. Tusha, A. Tusha, E. Basar, and H. Arslan, "Multidimensional index modulation for 5G and beyond wireless networks," *Proceedings of the IEEE*, vol. 109, no. 2, pp. 170–199, 2020.

[39] E. Basar, M. Wen, R. Mesleh, M. Di Renzo, Y. Xiao, and H. Haas, "Index modulation techniques for next-generation wireless networks," *IEEE access*, vol. 5, pp. 16 693–16 746, 2017.

[40] I. A. Hemadeh, M. El-Hajjar, S. Won, and L. Hanzo, "Multi-set space-time shift-keying with reduced detection complexity," *IEEE Access*, vol. 4, pp. 4234–4246, 2016.

[41] T. Mao, Q. Wang, Z. Wang, and S. Chen, "Novel index modulation techniques: A survey," *IEEE Communications Surveys & Tutorials*, vol. 21, no. 1, pp. 315–348, 2018.

[42] Q. Wang, W. Yang, S. Xu, and X. Pei, "OFDM with Index Modulation for UAV Communication Systems," in *2019 IEEE 5th International Conference on Computer and Communications (ICCC)*. IEEE, 2019, pp. 1047–1052.

[43] M. Xie, X. Yu, J. Chen, and T. Teng, "BER performance of unmanned aerial vehicle assisted spatial modulation system in Rician channels," *Physical Communication*, vol. 49, p. 101471, 2021.

[44] C. Xu, T. Bai, J. Zhang, R. Rajashekar, R. G. Maunder, Z. Wang, and L. Hanzo, "Adaptive coherent/non-coherent spatial modulation aided unmanned aircraft systems," *IEEE Wireless Communications*, vol. 26, no. 4, pp. 170–177, 2019.

[45] M. C. Taştan and H. İlhan, "Performance Analysis of SSK Modulation for UAVs Communication," *Vehicular Communications*, p. 100375, 2021.

[46] L. Qiao, J. Zhang, Z. Gao, D. Zheng, M. J. Hossain, Y. Gao, D. W. K. Ng, and M. Di Renzo, "Joint Activity and Blind Information Detection for UAV-Assisted Massive IoT Access," *IEEE Journal on Selected Areas in Communications*, vol. 40, no. 5, pp. 1489–1508, 2022.

[47] A. Fotouhi, H. Qiang, M. Ding, M. Hassan, L. G. Giordano, A. Garcia-Rodriguez, and J. Yuan, "Survey on UAV cellular communications: Practical aspects, standardization advancements, regulation, and security challenges," *IEEE Communications Surveys & Tutorials*, vol. 21, no. 4, pp. 3417–3442, 2019.

[48] T. Tomic, K. Schmid, P. Lutz, A. Domel, M. Kassecker, E. Mair, I. L. Grixa, F. Ruess, M. Suppa, and D. Burschka, "Toward a fully autonomous UAV: Research platform for indoor and outdoor urban search and rescue," *IEEE robotics & automation magazine*, vol. 19, no. 3, pp. 46–56, 2012.

[49] S. Ullah, K.-I. Kim, K. H. Kim, M. Imran, P. Khan, E. Tovar, and F. Ali, "UAV-enabled healthcare architecture: Issues and challenges," *Future Generation Computer Systems*, vol. 97, pp. 425–432, 2019.

[50] A. Younis, N. Serafimovski, R. Mesleh, and H. Haas, "Generalised spatial modulation," in *2010 conference record of the forty fourth Asilomar conference on signals, systems and computers*. IEEE, 2010, pp. 1498–1502.

[51] K. Seong, M. Mohseni, and J. M. Cioffi, "Optimal resource allocation for OFDMA downlink systems," in *2006 IEEE International Symposium on Information Theory*. IEEE, 2006, pp. 1394–1398.

[52] G. Li and H. Liu, "Downlink radio resource allocation for multi-cell OFDMA system," *IEEE transactions on wireless communications*, vol. 5, no. 12, pp. 3451–3459, 2006.

[53] I. C. Wong and B. L. Evans, "Optimal downlink OFDMA resource allocation with linear complexity to maximize ergodic rates," *IEEE Transactions on Wireless Communications*, vol. 7, no. 3, pp. 962–971, 2008.

[54] G. L. Stuber, J. R. Barry, S. W. Mclaughlin, Y. Li, M. A. Ingram, and T. G. Pratt, "Broadband MIMO-OFDM wireless communications," *Proceedings of the IEEE*, vol. 92, no. 2, pp. 271–294, 2004.

[55] L.-L. Yang, *Multicarrier communications*. John Wiley & Sons, 2009.

[56] J. Lyu, Y. Zeng, R. Zhang, and T. J. Lim, "Placement optimization of UAV-mounted mobile base stations," *IEEE Communications Letters*, vol. 21, no. 3, pp. 604–607, 2016.

[57] L. Liu, W. Hong, H. Wang, G. Yang, N. Zhang, H. Zhao, J. Chang, C. Yu, X. Yu, H. Tang *et al.*, "Characterization of line-of-sight MIMO channel for fixed wireless communications," *IEEE Antennas and Wireless Propagation Letters*, vol. 6, pp. 36–39, 2007.

[58] G. J. Foschini, "Layered space-time architecture for wireless communication in a fading environment when using multi-element antennas," *Bell labs technical journal*, vol. 1, no. 2, pp. 41–59, 1996.

[59] V. Erceg, P. Soma, D. S. Baum, and A. J. Paulraj, "Capacity obtained from multiple-input multiple-output channel measurements in fixed wireless environments at 2.5 ghz," in *2002 IEEE International Conference on Communications. Conference Proceedings. ICC 2002 (Cat. No. 02CH37333)*, vol. 1. IEEE, 2002, pp. 396–400.

[60] C. Tepedelenlioglu, A. Abdi, and G. B. Giannakis, "The Ricean K factor: estimation and performance analysis," *IEEE Transactions on Wireless Communications*, vol. 2, no. 4, pp. 799–810, 2003.

[61] S. Zhu, T. S. Ghazaany, S. M. Jones, R. A. Abd-Alhameed, J. M. Noras, T. Van Buren, J. Wilson, T. Suggett, and S. Marker, "Probability Distribution of Rician K-Factor in Urban, Suburban and Rural Areas Using Real-World Captured Data," *IEEE Transactions on Antennas and Propagation*, vol. 62, no. 7, pp. 3835–3839, 2014.

[62] P. Stoica, R. L. Moses *et al.*, "Spectral analysis of signals," 2005.

[63] S. Suman, S. Kumar, and S. De, "Path loss model for UAV-assisted RFET," *IEEE Communications Letters*, vol. 22, no. 10, pp. 2048–2051, 2018.

[64] T. S. Rappaport, "Mobile radio propagation: Large-scale path loss," *Wireless communications: principles and practice*, pp. 107–110, 2002.

[65] M. Zhang, Y. Xiong, S. X. Ng, and M. El-Hajjar, "Content-Aware Transmission in UAV-Assisted Multicast Communication," *IEEE Transactions on Wireless Communications*, 2023.

[66] B. S. Chaudhari and M. Zennaro, *LPWAN Technologies for IoT and M2M Applications*. Academic Press, 2020.

[67] L. Gupta, R. Jain, and G. Vaszkun, "Survey of important issues in UAV communication networks," *IEEE Communications Surveys & Tutorials*, vol. 18, no. 2, pp. 1123–1152, 2015.

[68] R. Amorim, H. Nguyen, P. Mogensen, I. Z. Kovács, J. Wigard, and T. B. Sørensen, "Radio channel modeling for UAV communication over cellular networks," *IEEE Wireless Communications Letters*, vol. 6, no. 4, pp. 514–517, 2017.

[69] E. Telatar, "Capacity of multi-antenna Gaussian channels," *European transactions on telecommunications*, vol. 10, no. 6, pp. 585–595, 1999.

[70] A. Goldsmith, S. A. Jafar, N. Jindal, and S. Vishwanath, "Capacity limits of MIMO channels," *IEEE Journal on selected areas in Communications*, vol. 21, no. 5, pp. 684–702, 2003.

[71] S. Vishwanath, N. Jindal, and A. Goldsmith, "Duality, achievable rates, and sum-rate capacity of Gaussian MIMO broadcast channels," *IEEE Transactions on information theory*, vol. 49, no. 10, pp. 2658–2668, 2003.

[72] A. A. Ibrahim, T. Kim, and D. J. Love, "On the achievable rate of generalized spatial modulation using multiplexing under a Gaussian mixture model," *IEEE Transactions on Communications*, vol. 64, no. 4, pp. 1588–1599, 2016.

[73] S. Ruder, "An overview of gradient descent optimization algorithms," *arXiv preprint arXiv:1609.04747*, 2016.

[74] K. B. Petersen, M. S. Pedersen *et al.*, "The matrix cookbook," *Technical University of Denmark*, vol. 7, no. 15, p. 510, 2008.

[75] S. Cui, A. J. Goldsmith, and A. Bahai, "Energy-constrained modulation optimization for coded systems," in *GLOBECOM'03. IEEE Global Telecommunications Conference (IEEE Cat. No. 03CH37489)*, vol. 1. IEEE, 2003, pp. 372–376.

[76] ——, "Modulation optimization under energy constraints," in *IEEE International Conference on Communications, 2003. ICC'03.*, vol. 4. IEEE, 2003, pp. 2805–2811.

[77] T. H. Lee, *The design of CMOS radio-frequency integrated circuits*. Cambridge university press, 2003.

[78] M. Parker, *Digital Signal Processing 101: Everything you need to know to get started*. Newnes, 2017.

[79] S. Cui, A. J. Goldsmith, and A. Bahai, "Energy-efficiency of mimo and cooperative mimo techniques in sensor networks," *IEEE Journal on selected areas in communications*, vol. 22, no. 6, pp. 1089–1098, 2004.

[80] M. Gustavsson, J. J. Wikner, and N. Tan, *CMOS data converters for communications*. Springer Science & Business Media, 2000, vol. 543.

[81] S. Cui, A. J. Goldsmith, and A. Bahai, "Energy-constrained modulation optimization," *IEEE transactions on wireless communications*, vol. 4, no. 5, pp. 2349–2360, 2005.

[82] Rohde-Schwarz. (2020) IEEE 802.11ax TECHNOLOGY INTRODUCTION. [Online]. Available: https://www.rohde-schwarz.com/uk/solutions/test-and-measurement/wireless-communication/wireless-connectivity/wlan-wifi/wlan-ieee-802.11ax-testing/white-paper-ieee-802.11ax-technology-introduction_253050.html

[83] T. L. Narasimhan and A. Chockalingam, "On the capacity and performance of generalized spatial modulation," *IEEE Communications Letters*, vol. 20, no. 2, pp. 252–255, 2015.

[84] C. M. Bishop, "Pattern recognition," *Machine learning*, vol. 128, no. 9, pp. 523–554, 2006.